Applied Catalysis B: Environmental 95 (2010) 26–38

Contents lists available at ScienceDirect

Applied Catalysis B: Environmental

journal homepage: www.elsevier.com/locate/apcatb

Kinetic modeling of the total oxidation of propane over CuO-CeO_2/γ-Al_2O_3

M. Philippe Heynderickx [a], Joris W. Thybaut [a,*], Hilde Poelman [a], Dirk Poelman [b], Guy B. Marin [a]

[a] Laboratory for Chemical Technology, Chemical Engineering Department, Ghent University, Krijgslaan 281-S5, Ghent, B-9000, Belgium
[b] Department of Solid State Sciences, LumiLab, Ghent University, Krijgslaan 281-S1, Ghent, B-9000, Belgium

ARTICLE INFO

Article history:
Received 14 August 2009
Received in revised form 26 November 2009
Accepted 30 November 2009
Available online 21 December 2009

Keywords:
Total oxidation
Kinetics
Modeling
Langmuir–Hinshelwood
Eley–Rideal
Mars–van Krevelen

ABSTRACT

The total oxidation of propane is studied by means of steady-state experiments over a CuO-CeO_2/γ-Al_2O_3 catalyst at propane inlet partial pressures of 0.2–1.0 kPa, oxygen inlet partial pressures of 2.7–27.6 kPa and temperatures from 543 to 648 K. The inlet ratio of oxygen to propane is varied between 6.1 and 28.0 $mol_{O_2,0}\,mol^{-1}_{C_3H_8,0}$. Water and carbon dioxide inlet partial pressures up to 12.4 kPa are investigated. The complete experimental dataset was regressed with a priori possible Langmuir–Hinshelwood (LH), Eley–Rideal (ER) and Mars–van Krevelen (MVK) rate equations. A LH rate equation, the rate-determining step being the surface reaction between one adsorbed propane species and one dissociatively adsorbed oxygen species, allows the best description of the data.

The surface reaction activation energy amounts to 74.4 ± 4.6 kJ mol^{-1}. All adsorption steps in the selected reaction mechanism are quasi-equilibrated. The values of the preexponential factors of the adsorption equilibrium coefficients correspond to rather mobile surface species. Molecular water adsorption is followed by a dissociation of the adsorbed water by interaction with a dissociatively adsorbed oxygen species to form two hydroxyl species.

1. Introduction

Volatile organic compounds (VOCs) exhibit a significant vapour pressure at ambient conditions. These compounds are responsible for increasing levels of ozone in the troposphere and for ozone depletion in the stratosphere. Emissions from both stationary and non-stationary sources are subjected to an ever stricter legislation, due to an increasing environmental awareness. According to Theloke and Friedrich [1], four main sources of VOC can be distinguished, namely transport (37%), solvent use (55%), production and storage processes (4%) and combustion processes (4%). From all these sources, one third of all emitted gases are alkanes.

One possible way to reduce the VOC emission is catalytic oxidation on heterogeneous transition metal oxide catalysts [2]. Catalytic oxidation offers the advantage that these VOCs can be removed from effluent streams with low concentration at relatively low temperatures. Furthermore, the advantage of using catalysts based on transition metal oxides, rather than on noble metals, is associated with their lower cost, possible higher thermal stability and greater resistance to poisoning [3].

This work investigates the kinetics of the total oxidation of propane as a VOC model molecule over a CuO-CeO_2/γ-Al_2O_3 catalyst by means of steady-state experiments. This catalyst is taken as a typical catalyst for total oxidation reactions. Experimental specific reaction rates in the range 10^{-4} – 10^{-3} $mol_{C_3H_8}\,kg^{-1}_{cat}\,s^{-1}$ are obtained, vide infra, which are comparable to those, obtained with other metal oxide catalysts in propane total oxidation [4–6].

The ultimate goal is to identify the most appropriate kinetic model for the total oxidation of propane based on steady-state data. To this purpose, 69 a priori possible kinetic models have been constructed and evaluated. This approach, albeit for a lower number of kinetic models, has been successfully applied before [7–14]. Analysis of the initial reaction rates, comparison of experimental and theoretical partial reaction orders and transformation of the non-linear rate expressions into a set of equations, linear in the parameters to be estimated, constitute the basis for an isothermal model discrimination. Non-isothermal parameter estimation is performed for the selected models and final model discrimination is realized by application of the so-called 'likelihood criterion'. Model refinement with respect to the adsorption behaviour of water is performed by considering a more detailed interaction between oxygen and water derived surface species, all of them considered to be quasi-equilibrated.

Abbreviations: DOF, degrees of freedom; ER, Eley–Rideal; GC, gas chromatograph; LH, Langmuir–Hinshelwood; MVK, Mars–van Krevelen; NLV, number of lumped variables; NLP, number of lumped parameters; VOC, volatile organic compound.

* Corresponding author.
E-mail address: Joris.Thybaut@UGent.be (J.W. Thybaut).

0926-3373/$ – see front matter © 2009 Elsevier B.V. All rights reserved.
doi:10.1016/j.apcatb.2009.11.018

Nomenclature

a_v	surface area to volume of a particle ($m^2\ m^{-3}$)
A	constant in Eqs. (2) and (S-10) ($mol_{C_3H_8}\ mol^{-1}_{C_3H_8,0}$)
A'_i	logarithm of preexponential factor, used in Eq. (15) ($mol_{C_3H_8}\ kg^{-1}_{cat}\ s^{-1}$)
A_i	surface area of the peak of component i (V s)
b	volume of inert material as fraction of total solid ($m^3\ m^{-3}$)
b_i	parameter estimate, group of lumped parameters (dep.)
B	constant in Eqs. (2) and (S-10) ($mol_{C_3H_8,0}\ kg^{-1}_{cat}\ s^{-1}$)
Bo	Bodenstein number ($= u_s d_p / D_{C_3H_8,ax}$) (–)
C_i	concentration of component i ($mol\ m^{-3}$)
d_i	calibration factor for component i ($V\ s\ mol^{-1}$)
d_p	particle diameter (m)
d_t	reactor tube diameter (m)
D	diffusion coefficient ($m^3\ m^{-1}\ s^{-1}$)
E_A	activation energy ($kJ\ mol^{-1}$)
F_i	molar flow rate of component i ($mol\ s^{-1}$)
F_m	calculated F value for model m (–)
$-\Delta H^\circ$	standard enthalpy ($kJ\ mol^{-1}$)
$-\Delta_r H^\circ$	standard reaction enthalpy ($kJ\ mol^{-1}$)
k	reaction rate coefficient (dep.)
k_s	surface reaction rate coefficient ($mol_{C_3H_8}\ kg^{-1}_{cat}\ s^{-1}$)
$k_{C_3H_8}$	rate coefficient for reduction ($mol_{C_3H_8}\ kg^{-1}_{cat}\ s^{-1}\ kPa^{-1}$)
k_{CO_2}	rate coefficient for irreversible desorption of carbon dioxide ($mol_{C_3H_8}\ kg^{-1}_{cat}\ s^{-1}$)
k_g	mass transfer coefficient from gas to solid interface ($m^3\ m^{-2}\ s^{-1}$)
k_{H_2O}	rate coefficient for irreversible desorption of water ($mol_{C_3H_8}\ kg^{-1}_{cat}\ s^{-1}$)
k_{O_2}	rate coefficient for reoxidation ($mol_{C_3H_8}\ kg^{-1}_{cat}\ s^{-1}\ kPa^{-1}$)
k'_{O_2}	rate coefficient for step 14 in Table S-2 (–)
K_i	adsorption equilibrium coefficient for component i (kPa^{-1})
L	catalyst bed length (m)
m^*	number of oxygen species, involved in a surface reaction, vide Eq. (6) (–)
M	number of coupled algebraic equations (–)
n	partial reaction order, number of experimental points, number of parameters (–)
n_i	number of carbon atoms in component (–)
n_j	number of experiments on temperature level j (–)
n^*	characteristic number for oxygen adsorption, vide Eq. (6) (–)
N	adsorption group (–)
N_C	number of carbon containing components (–)
N_T	number of temperature levels (–)
p	number of parameters (–)
p_i	partial pressure of component i (kPa)
ΔP	pressure drop (kPa)
r	specific reaction rate ($mol_{C_3H_8}\ kg^{-1}_{cat}\ s^{-1}$)
R	universal gas constant ($kJ\ mol^{-1}\ K^{-1}$)
s	number of duplicated experiments (–)
$s^2_{j,m}$	mean square of the residuals on temperature level j, vide Eq. (18) ($mol^2\ mol^{-2}$)
S	gas phase entropy ($J\ mol^{-1}\ K^{-1}$)
S_m	residual sum of squares in model m ($mol^2\ mol^{-2}$)
S_m^*	pure-error sum of squares for model m ($mol^2\ mol^{-2}$)
$-\Delta S'_i 0$	standard entropy for component i, used in Eq. (16) ($kJ\ mol^{-1}\ K^{-1}$)
$-\Delta S^\circ$	standard entropy ($J\ mol^{-1}\ K^{-1}$)
t	t value (–)
T	temperature (K)
u	gas phase velocity ($m\ s^{-1}$)
$V(b_{ii})$	i^{th} diagonal element in the covariance matrix (dep.)
$w_{j,m}$	weight factor for model m on temperature level j ($mol\ mol^{-1}$)
W_{cat}	mass of catalyst loaded (kg_{cat})
x_i	group of lumped variables (dep.)
y_i	group of lumped variables (dep.)
$X_{C_3H_8}$	fractional propane conversion ($mol_{C_3H_8}\ mol^{-1}_{C_3H_8,0}$)

Greek letters

α	confidence level (–)
α	heat transfer coefficient between pellet and gas phase ($kJ\ m^{-2}\ K^{-1}\ s^{-1}$)
β_i	parameter i (dep.)
γ	ratio of oxygen and propane partial pressure $mol_{O_2}\ mol^{-1}_{C_3H_8}$
ε	porosity ($m^3\ m^{-3}$)
θ	fractional coverage (–)
λ	catalyst conductivity ($kJ\ m^{-1}\ K^{-1}\ s^{-1}$)
Λ	variable, used in Section S.4 (–)
μ	dynamic viscosity ($kg\ m^{-1}\ s^{-1}$)
ρ	density ($kg\ m^{-3}$)
σ	stoichiometric number (–)

Subscripts

ad	adequacy
ads	adsorption
ax	axial
b	bed, bulk
calc	calculated
diss	dissociation
eff	effective
f	fluid
g	gas phase
i	component i
j	temperature level j
m	number of kinetic model m
max	maximum
min	minimum
obs	observed
p	particle
s	surface, superficial
sig	significance
tab	tabulated
t	total
w	wall
0	inlet, initial

_	vector
=	matrix
Superscripts	
–	average
^	calculated
′	modified
*	reference, adsorbed species
0	standard

2. Procedures

2.1. Catalyst

A commercial CuO-CeO_2/γ-Al_2O_3 catalyst, prepared by impregnation [15,16], is used. From ICP measurements, it has been calculated that the catalyst contains $1.46\,mol_{Cu}\,kg_{cat}^{-1}$ and $0.37\,mol_{Ce}\,kg_{cat}^{-1}$. A specific surface area of $1.56 \times 10^{+5}\,m^2\,kg_{cat}^{-1}$ is obtained from N_2 physisorption in a Micromeritics Gemini instrument [9].

2.2. Steady-state experiments

2.2.1. Experimental

The evaluation of the catalytic activity in the total oxidation of propane is carried out in a conventional fixed-bed reactor with inner diameter of 1.4×10^{-2} m, using 2 g of catalyst, diluted with 10 g of quartz. The particle diameter is in the range 4.0–5.0×10^{-4} m. Steady-state experiments are performed at the conditions mentioned in Table 1. In order to evaluate the catalytic activity in the presence of reaction products, mixtures with water or carbon dioxide are fed over the catalyst bed. A blank experiment at the most severe experimental conditions, i.e., $p_{C_3H_8,0} = 1.0$ kPa, $p_{O_2,0} = 27.6$ kPa, $p_{H_2O,0} = p_{CO_2,0} = 0.0$ kPa, $W_{cat}F_{C_3H_8,0}^{-1} = 173\,kg_{cat}\,s\,mol_{C_3H_8,0}^{-1}$ and $T = 648$ K, over inert material shows no propane conversion. The isothermicity of the catalyst bed is guaranteed by three experimental interventions: the reactor was placed in a molten salt bath, which ensures a very high heat transfer, transporting the heat of reaction [17]; the catalyst bed was diluted with inert quartz, ratio 1:5; and the inlet molar fraction of propane never exceeded 0.01 $mol_{C_3H_8,0}\,mol_{t,0}^{-1}$. Within the specified range of experimental conditions, given in Table 1, 377 experimental conditions are set. The propane conversion ranges from 0.01 up to 0.87 $mol_{C_3H_8}\,mol_{C_3H_8,0}^{-1}$.

Criteria for the establishment of the plug flow regime as well as for the absence of concentration and temperature gradients on pellet and reactor scale have been assessed [18]. The catalyst bed length is 3.5×10^{-2} m with a bed porosity of 0.41 $m^3\,m^{-3}$. An effective diffusion coefficient of $6.7 \times 10^{-7}\,m^2\,s^{-1}$ and a tortuosity of 2.0 $m^2\,m^{-2}$ for the porous catalysts is used. The heat of propane total oxidation reaction is $2.0 \times 10^{+6}\,J\,mol^{-1}$.

Table 1
Range of experimental conditions during the steady-state total oxidation of propane over CuO-CeO_2/γ-Al_2O_3. Helium is used as balance gas.

Process condition	Unit	Range
$p_{C_3H_8,0}$	/kPa	0.2–1.0
$p_{O_2,0}$	/kPa	2.7–27.6
$p_{H_2O,0}$	/kPa	0.0–11.1
$p_{CO_2,0}$	/kPa	0.0–12.4
$\gamma_0 = y_{O_2,0}y_{C_3H_8,0}^{-1}$	$/mol_{O_2,0}\,mol_{C_3H_8,0}^{-1}$	6.1–28.0
$W_{cat}F_{C_3H_8,0}^{-1}$	$/kg_{cat}\,s\,mol_{C_3H_8,0}^{-1}$	173–570
T	/K	543–648
$X_{C_3H_8}$	$/mol_{C_3H_8}\,mol_{C_3H_8,0}^{-1}$	0.01–0.87

For a maximal initial specific reaction rate of 3.8×10^{-3} $mol\,kg_{cat}^{-1}\,s^{-1}$, a maximum reaction temperature of 648 K, a maximum propane conversion of 0.87 $mol\,mol^{-1}$ and a maximum activation energy for propane combustion of 90.0 $kJ\,mol^{-1}$ these criteria are verified. It can be shown, vide Section S.1, that a plug-flow regime is established and that concentration and temperature gradients on pellet as well as on reactor scale can be neglected. Hence, all experimental data points are acquired in the intrinsic kinetic regime.

The steady-state continuity equation for propane is given by Eq. (1) with the initial condition that $X_{C_3H_8} = 0\,mol_{C_3H_8}\,mol_{C_3H_8,0}^{-1}$ for $W_{cat}/F_{C_3H_8,0} = 0\,kg_{cat}\,s\,mol_{C_3H_8,0}^{-1}$.

$$\frac{dX_{C_3H_8}}{d(W_{cat}/F_{C_3H_8,0})} = r \tag{1}$$

From an empirical relation between the propane conversion and the space time [19], vide Eq. (2), the initial specific reaction rate is obtained via Eq. (1) at zero space time and is given by the product AB. Eq. (2) represents the propane conversion, corresponding to a first order reaction, $r = kC_{C_3H_8}$, if $A = 1$ and $B = kC_{C_3H_8,0}$. Additionally, a modification parameter, $A \neq 1$, is introduced in order to account for non-integer partial reaction order:

$$X_{C_3H_8} = A\left(1 - \exp\left(-B\frac{W_{cat}}{F_{C_3H_8,0}}\right)\right) \tag{2}$$

2.2.2. Analysis

Effluent gases are analyzed on-line using a GC 8000 gas chromatograph (Interscience) with a thermal conductivity detector, using methane as internal standard. The only products formed are water and carbon dioxide. No partial oxidation products such as propene or carbon monoxide are detected in the reactor effluent mixture. The conversion of propane is calculated using the normalization method, vide Eq. (3), in which A_i and d_i represent the surface area obtained for component i in the chromatogram and the corresponding calibration factor; n_i is the number of carbon atoms in component i and N_C is the number of carbon containing components in the reactor effluent. Only the experiments in which the carbon balance is closed within 5% are retained for further processing.

$$X_{C_3H_8} = \frac{\sum_{\substack{i=1 \\ i \neq C_3H_8}}^{N_C} n_i A_i/d_i}{\sum_{i=1}^{N_C} n_i A_i/d_i} \tag{3}$$

3. Kinetic modeling: procedures and methodology

3.1. List of a priori possible kinetic models

A power law reaction rate expression, as given by Eq. (4), is used to obtain a preliminary dependency on the propane and oxygen partial pressures, vide Section 4.

$$r = k\,p_{C_3H_8}^{n_{C_3H_8}}\,p_{O_2}^{n_{O_2}} \tag{4}$$

Besides a power law rate expression, three types of reaction mechanisms are considered: Langmuir–Hinshelwood (LH), Eley–Rideal (ER) and Mars–van Krevelen (MVK). The distinctive features between these mechanisms are related to the rate-determining step that is considered, the adsorption of reactants and products or reaction from the gas phase, the number of chemisorbed oxygen species involved in the rate-determining

Table 2
Elementary steps and reaction path for C_3H_8 total oxidation by O_2 over CuO-CeO_2/γ-Al_2O_3 in the presence of reaction products. A free surface site is represented by * and an adsorbed atom of molecule *X* by *X**.

Step number	Elementary step		Reaction path	
			LH18	LH*2
1	$C_3H_8 + * \rightleftharpoons C_3H_8^*$	$K_{C_3H_8} = \frac{\theta_{C_3H_8^*}}{p_{C_3H_8}\theta_*}$	1	1
2	$O_2 + 2* \rightleftharpoons 2O^*$	$K_{O_2} = \frac{\theta_{O^*}^2}{p_{O_2}\theta_*^2}$	5	5
3	$C_3H_8^* + O^* \dashrightarrow \ldots \xrightarrow{+9O^*} 3CO_2^* + 4H_2O^* + 4*$	$r = k_s\theta_{C_3H_8^*}\theta_{O^*}$	1	1
4	$H_2O^* \rightleftharpoons H_2O + *$	$K_{H_2O}^{-1} = \frac{p_{H_2O}\theta_*}{\theta_{H_2O^*}}$	4	4
5	$2HO^* \rightleftharpoons H_2O^* + O^*$	$K_{diss,2}^{-1} = \frac{\theta_{H_2O^*}\theta_{O^*}}{\theta_{HO^*}^2}$	–[a]	0[b]
6	$CO_2^* \rightleftharpoons CO_2 + *$	$K_{CO_2}^{-1} = \frac{p_{CO_2}\theta_*}{\theta_{CO_2^*}}$	3	3
+	$C_3H_8 + 5O_2 \rightarrow 3CO_2 + 4H_2O$			

[a] the dissociation of water on the catalyst surface is not considered in LH18.
[b] the dissociation of adsorbed water is considered in LH*2 resulting in the formation of HO* species. Mathematically, the latter species are spectator molecules resulting in a stoichiometric parameter of 0 for this reaction step in the overall reaction path.

step, the effect of reaction products and the number of types of active sites.

In this work, the effects of reaction products will in first instance be accounted for by considering a quasi-equilibrated associative adsorption of water and carbon dioxide, vide Sections 3.1.1 and 3.1.2. If the corresponding desorption steps would be rate-determining, the reaction rate would be independent of the applied inlet partial pressures at every temperature level [20,21]. This is experimentally not observed, vide Section 5.2. The complete list of a priori possible kinetic models is given in Table S-3, vide Section S.2.

It has to be noted that the surface species, formed after the surface reaction step, e.g., step 3 in Table 2, are not incorporated in the reaction mechanism. The subsequent surface reactions, giving finally rise to adsorbed products, are considered to be potentially very fast and, hence, kinetically irrelevant [22], vide Eq. (5). In alkane oxidation reactions, it is indeed generally accepted [23–36] that the activation of the alkane is the most difficult step. The surface reaction step, vide Eq. (5), represents the activation of the adsorbed propane by reaction with a dissociatively adsorbed oxygen species and, hence, this step is considered to be the rate determining step:

$$C_3H_8^* + O^* \dashrightarrow \ldots \quad (5)$$

This approach will lead to the selection of a reaction rate expression. The latter will then be refined by considering in a more detailed way the interaction of water with the catalyst, vide Section 6.

3.1.1. Langmuir–Hinshelwood (LH) mechanisms

LH mechanisms consider the adsorption of both reactants on the catalyst surface. For models LH1 to LH6, the propane adsorption is the rate-determining step. Oxygen adsorption is considered to be the rate-determining step in models LH7 to LH12. In these rate expressions, the distinctive features are the associative or dissociative adsorption of oxygen. If the reaction products are present in non-negligible amounts on the catalyst surface, additional adsorption terms are added in the denominator. This is of particular importance for water, which is reported to strongly adsorb on metal oxide catalysts [7,13,37]. In this respect, one additional adsorption term for water is added, corresponding to a competitive adsorption of reactants and water, formed in the total oxidation reaction. If both reaction products occupy a significant fraction of active sites, two adsorption terms are added in the denominator. In the further development of possible models for total oxidation of propane over a CuO-CeO_2/γ-Al_2O_3 catalyst, the incorporation of additional adsorption terms for water and carbon dioxide is done in a similar way.

Models LH13 to LH44, having as common feature that the surface reaction is rate determining, differ amongst each other in the number of associatively or dissociatively chemisorbed oxygen species, the number of types of active sites. Rate expressions LH13 to LH24, where the adsorption of reactant molecules and the surface reaction takes place on one type of active site, can be generally represented by Eq. (6), in which n^* is determined by the type of oxygen adsorption, i.e., $n^* = 1$ corresponds to dissociative and $n^* = 2$ to molecular adsorption, and m^* reflects the number of oxygen species, involved in the rate-determining step. An example of elementary reaction steps, corresponding to $n^* = 2$ and $m^* = 1$, is given in Table 2. When the reaction products do not occupy a significant fraction of active sites, the corresponding adsorption terms can be removed from the rate expression (6).

$$r = k_s \frac{(K_{O_2} p_{O_2})^{m^* n^*/2} K_{C_3H_8} p_{C_3H_8}}{(1 + (K_{O_2} p_{O_2})^{n^*/2} + K_{C_3H_8} p_{C_3H_8} + K_{H_2O} p_{H_2O} + K_{CO_2} p_{CO_2})^{1+m^*}} \quad (6)$$

Models LH25 to LH44 take into account the presence of two types of active sites. This is not uncommon, since the metal oxide catalyst is constituted of two active phases, i.e., CuO and CeO_2. Oxygen can adsorb molecularly or dissociatively on one type of active site, whereas propane can adsorb on the other type of site. One or two adsorbed oxygen species can be involved in the surface reaction and the reaction products can occupy a fraction of one type of active sites. An example of a competitive-adsorption rate expression is given by Eq. (7):

$$r = k_s \frac{(K_{O_2} p_{O_2})^{m^* n^*/2} K_{C_3H_8} p_{C_3H_8}}{(1 + K_{C_3H_8} p_{C_3H_8})(1 + (K_{O_2} p_{O_2})^{n^*/2} + K_{H_2O} p_{H_2O} + K_{CO_2} p_{CO_2})^{m^*}} \quad (7)$$

3.1.2. Eley–Rideal (ER) mechanisms

In the case of an ER mechanism, one reactant adsorbs on the catalyst surface and the other one reacts directly from the gas phase with the adsorbed reactant. When propane adsorbs on the catalyst, rate expressions ER1 to ER3 are obtained. When oxygen

adsorbs associatively or dissociatively, expressions ER4 to ER15 are derived. A general expression for the latter models is given by Eq. (8):

$$r = k_s \frac{(K_{O_2} p_{O_2})^{m^* n^*/2} p_{C_3H_8}}{(1 + (K_{O_2} p_{O_2})^{n^*/2} + K_{H_2O} p_{H_2O} + K_{CO_2} p_{CO_2})^{m^*}} \quad (8)$$

3.1.3. Mars–van Krevelen (MVK) mechanisms

Ten MVK models are added to list of kinetic models. Model MVK1, vide Eq. (9), is constructed according to a mechanism involving a reduction step, with rate coefficient $k_{C_3H_8}$, in which propane reacts with a single oxidized site and with a reoxidation step, with rate coefficient k_{O_2}, by gas phase oxygen, involving a single reduced site. The factor '5' in the denominator of the corresponding rate equation originates from the number of oxygen molecules needed in the total oxidation of one propane molecule [38].

$$r = \frac{k_{O_2} k_{C_3H_8} p_{O_2} p_{C_3H_8}}{k_{O_2} p_{O_2} + 5 k_{C_3H_8} p_{C_3H_8}} \quad (9)$$

When the desorption of reaction products is accounted for, the combination of the corresponding steady-state reaction rates, vide Eq. (10), and the balance for the active sites, Eq. (11), results in Eq. (12):

$$r = k_{C_3H_8} p_{C_3H_8} \theta_{O^*} = \frac{1}{5} k_{O_2} p_{O_2} \theta_* = \frac{1}{3} k_{CO_2} \theta_{CO_2^*} = \frac{1}{4} k_{H_2O} \theta_{H_2O^*} \quad (10)$$

$$\theta_{O^*} + \theta_* + \theta_{CO_2^*} + \theta_{H_2O^*} = 1 \quad (11)$$

$$r = \frac{k_{O_2} k_{C_3H_8} p_{O_2} p_{C_3H_8}}{k_{O_2} p_{O_2} + 5 k_{C_3H_8} p_{C_3H_8} + k_{O_2} k_{C_3H_8} p_{O_2} p_{C_3H_8} [4/k_{H_2O} + 3/k_{CO_2}]} \quad (12)$$

Since no explicit partial pressure dependency of reaction products is present in Eq. (12), this contribution is often lumped in one rate coefficient k_P and an average stoichiometric number ν_P, vide Eq. (13). For example, in the total oxidation of methane, Hurtado et al. [37] put $\nu_P = 2$. In this work, no specific value is ascribed to ν_P and k_P/ν_P is estimated as a single parameter. Using Eqs. (10)–(13), rate expression MVK2, vide Table S-3, is obtained.

$$\frac{\nu_P}{k_P} = \frac{4}{k_{H_2O}} + \frac{3}{k_{CO_2}} \quad (13)$$

Model MVK3 describes the irreversible associative adsorption of oxygen, followed by its dissociation. Model MVK4 expresses that the reduction uses two oxidized sites from the catalyst surface. It is assumed in model MVK5 that the reoxidation involves gas phase oxygen and two reduced surface sites. Models MVK1 to MVK5 have already been reported in previous studies [7,37,39]. In model MVK6 two oxidized sites are used in the reduction step and the reoxidation involves gas phase oxygen and two reduced surface sites. This model was successfully applied by Arena et al. [28,29,30].

The MVK mechanism does not support reversible steps in the original proposition of this reaction mechanism [41] and, hence, taking into account the quasi-equilibrated adsorption of water and or carbon dioxide is not explicitly performed. In order to consider explicitly the possible partial pressure dependency of reaction products, vide Eq. (12), additional MVK models are proposed, vide Eqs. 67–69 in Table S-3: Eqs. 66 and 67, respectively, MVK7 and MVK8, represent the quasi-equilibrated adsorption of water and carbon dioxide on reduced sites, whereas Eqs. 68 and 69, respectively, MVK9 and MVK10, represent the quasi-equilibrated adsorption of reaction products on reoxidized sites. The former two rate expressions stem from the relations $\theta_{H_2O^*} = K_{H_2O} p_{H_2O} \theta_*$ and $\theta_{CO_2^*} = K_{CO_2} p_{CO_2} \theta_*$ [7]. For example, MVK8 is given by Eq. (14):

$$r = \frac{k_{O_2} k_{C_3H_8} p_{O_2} p_{C_3H_8}}{k_{O_2} p_{O_2} (1 + K_{H_2O} p_{H_2O} + K_{CO_2} p_{CO_2}) + 5 k_{C_3H_8} p_{C_3H_8}} \quad (14)$$

This type of kinetic models, specifically incorporating adsorption terms, is also used in total oxidation reactions by Barresi et al. [42,43], Hurtado et al. [44] and Ordoñez et al. [45].

The complete set of 69 kinetic models is listed in Table S-3, vide section S.3. Next, the best model for the total oxidation of propane over a $CuO\text{-}CeO_2/\gamma\text{-}Al_2O_3$ catalyst is selected.

3.2. Modeling and regression analysis: methodology

The selection of the best model in the total oxidation of propane over a $CuO\text{-}CeO_2/\gamma\text{-}Al_2O_3$ catalyst and the corresponding parameter estimation procedure consists of three main parts: initial reaction rate analysis, application of a transformation procedure, proposed by Barnard and Mitchell [46,47] and a non-isothermal parameter estimation. The kinetic parameters are subsequently assessed in terms of the physico-chemical meaningfulness of the corresponding parameter estimates.

3.2.1. Initial rate analysis

For a set of conditions with an identical ratio of oxygen and propane inlet partial pressures, γ_0, experimental initial specific reaction rates are obtained at five temperature levels, vide Section 2.2.1. By setting $p_{O_2,0} = \gamma_0 p_{C_3H_8,0}$, a set of theoretical initial specific reaction rate curves versus propane inlet partial pressure is constructed, based on the proposed models in Table S-3. By comparing the experimental and theoretical initial specific reaction rate curves, it is possible to rule out kinetic models.

3.2.2. Transformation procedure

A second step in the modeling and regression analysis is the application of a transformation procedure, proposed by Barnard and Mitchell [46]. This procedure, explained in the supplementary content, vide section S.3, tries to fit transformed parameters to transformed experimental data, in such a way that a set of equations, linear in the parameters to be estimated, is obtained. For each temperature level, the transformation procedure results in a unique solution allowing to avoid divergence problems in non-linear parameter estimation procedures. It can be shown that for the proposed rate equations the transformed parameters have to be non-negative values. If one of the transformed parameters is not estimated significantly different from zero, this statistically corresponds to setting this element to zero. This would imply that one of the real kinetic parameters is zero or infinite, which is not possible. An example is given in Section S.3.

If the transformed set of parameters only contains significantly estimated positive elements, the next step in the parameter estimation process can be performed. The given transformation procedure is successfully used by Wierzchowski and Zatorski in their determination of the kinetics in carbon monoxide and methane combustion over alumina supported catalysts [48].

The transformed parameters obtained in the above described procedure are used to calculate initial guesses of the actual kinetic parameters for the isothermal analysis of the experimental data.

3.2.3. Non-isothermal parameter estimation

A final step is the non-isothermal parameter estimation in which all experimental data are simultaneously used. Initial guesses for the preexponential factors, activation energies and adsorption enthalpies are obtained from Arrhenius diagrams constructed after the previous isothermal analysis. Reparameterization of rate coefficients and adsorption coefficients is done according to Eqs. (15) and (16), respectively. The reference temperature T^* is a number-averaged reaction temperature. By this means, binary correlation between preexponential factors and activation energies is reduced [49]. The absolute value of this correlation coefficient should not exceed 0.95 to avoid any significant correlation between the two corresponding parameters.

$$k_i = \exp\left[A'_i - \frac{E_{A,i}}{R}\left(\frac{1}{T} - \frac{1}{T^*}\right)\right] \tag{15}$$

$$K_j = \exp\left[\frac{\Delta S'^{\circ}_j}{R} - \frac{\Delta H^{\circ}_j}{R}\left(\frac{1}{T} - \frac{1}{T^*}\right)\right] \tag{16}$$

Using Eqs. (15) and (16), a weighted non-isothermal regression analysis is performed by the minimization of the objective function S_m, given by Eq. (17), corresponding to model m [50]. Propane conversion is used as response. The objective function is based upon the assumption that the experimental errors are normally distributed with a zero mean. This is verified by means of replicated experiments [51], vide Section S.5

$$S_m = \sum_{j=1}^{N_T} w_{j,m} \sum_{i=1}^{n_j} \left(X_{i,j} - \hat{X}_{i,j,m}\right)^2 \rightarrow \min \tag{17}$$

The weighting factor corresponding to every temperature level and model m is given by Eq. (18), in which the mean square of the residuals $s^2_{j,m}$ is defined by Eq. (19). It is assumed that the residuals are not correlated, since different catalytic measurements can be assumed to be stochastically independent.

$$w_{j,m} = \frac{1}{\sqrt{s^2_{j,m}}} \tag{18}$$

$$s^2_{j,m} = \frac{\sum_{i=1}^{n_j} (X_{i,j} - \hat{X}_{i,j,m})^2}{n_j - p} \tag{19}$$

Every parameter estimate is tested for its statistical significance using its individual t value, given by Eq. (20). A parameter is estimated significantly different from zero when its individual t value is higher than the corresponding tabulated value, given by $t_{\text{tab}}(n-p;\ 1-\alpha/2)$. A high individual t value indicates that the model calculations are very sensitive to the corresponding parameter. The corresponding confidence interval is obtained from Eq. (21).

$$(t_i)_{\text{calc}} = \frac{b_i}{\sqrt{V(\underline{b})_{ii}}} \tag{20}$$

$$b_i - t_{\text{tab}}\left(n-p,\ 1-\frac{\alpha}{2}\right)\sqrt{V(\underline{b})_{ii}} \le \beta_i \le b_i + t_{\text{tab}}\left(n-p,\ 1-\frac{\alpha}{2}\right)\sqrt{V(\underline{b})_{ii}} \tag{21}$$

The global significance of the non-isothermal regression is expressed by Fisher's F-test [49]. In this test the regression sum of squares and the residual sum of squares are compared. The degrees of freedom, DOF, corresponding to the latter are $\sum_{j=1}^{N_T} n_j - p$. A high calculated F value for model m, given by Eq. (22), corresponds to a high significance of the global regression of this model.

$$(F_m)_{\text{sig,calc}} = \frac{\sum_{j=1}^{N_T} w_{j,m} \sum_{i=1}^{n_j} \hat{X}^2_{i,j,m}\text{DOF}}{pS_m} \tag{22}$$

The relative model performance in a set of globally significant kinetic models can be evaluated using the so-called 'likelihood ratio' [21]. The latter is defined as the ratio of the joint probability density functions evaluated at the maximum-likelihood estimate. It is used as a selection criterion between rival kinetic models.

A kinetic model m is adequate when the calculated value $(F_m)_{\text{ad,calc}}$, vide Eq. (23), is smaller than the tabulated F value $F_{\text{tab}}(p, n-p;\ 1-\alpha)$ for a confidence level α, corresponding to p and $n-p$ degrees of freedom in the numerator and denominator respectively. The lack-of-fit sum of squares equals the residual sum of squares, S_m, minus the pure-error sum of squares, $S_m{}^*$, given by Eq. (24). The corresponding degrees of freedom, DOF*, are $\sum_{k=1}^{s}\sum_{j=1}^{N_T} n_{j,k^{-2}}$ and the average propane conversion, $\bar{X}_{j,k}$, corresponding to the kth replicate experiment on temperature level j, is given by Eq. (25).

$$(F_m)_{\text{ad,calc}} = \frac{S_m - S^*_m\text{DOF}}{(\text{DOF} - \text{DOF}^*)S^*_m} \tag{23}$$

$$S^*_m = \sum_{k=1}^{s}\sum_{j=1}^{N_T} w_{j,m} \sum_{i=1}^{n_{j,k}} (X_{i,j,k} - \bar{X}_{j,k})^2 \tag{24}$$

$$\bar{X}_{j,k} = \sum_{i=1}^{n_{j,k}} X_{i,j,k} \quad j = 1 \ldots N_T, k = 1 \ldots s \tag{25}$$

3.2.4. Assessment of the kinetic parameter estimates

Next to the individual significance of the model parameters and the global significance of the regression, physico-chemical tests such as Eqs. (26) and (27), are performed in order to determine whether the values of adsorption and desorption entropies have any physical meaning [52]. Eq. (26) indicates that the adsorption on the catalyst physically involves a loss of entropy and that it cannot be greater than the gas phase entropy. However, the entropy loss should be greater than 41.9 J mol^{-1} K^{-1}. Eq. (27) is an empirical rule [53] and it expresses that a more tightly bound molecule, corresponding to a larger negative value $-\Delta H^{\circ}_{\text{ads}}$, will be more restricted in its surface motion and the corresponding negative loss of entropy, $-\Delta S^{\circ}_{\text{ads}}$, will be larger.

$$41.9 < -\Delta S^{\circ}_{\text{ads}} < S^{\circ}_g \tag{26}$$

$$-\Delta S^{\circ}_{\text{ads}} \le 51.1 - 1.4\Delta H^{\circ}_{\text{ads}} \tag{27}$$

Violation of either of these two physico-chemical tests indicates inconsistencies in the proposed kinetic model and, hence, the estimated values for the adsorption parameters have no physical meaning in the Langmuirian sense. The standard gas phase entropy for oxygen and propane is respectively 342 and 227 J mol^{-1} K^{-1} at T^* = 617 K [54]. For water and carbon dioxide 246 and 214 J mol^{-1} K^{-1} are calculated.

The order of magnitude for the preexponential factors for LH surface reactions, given by Dumesic et al. [55], is expected to range from $8.5 \times 10^{+3}$ to $8.5 \times 10^{+8}$ $\text{mol}_{C_3H_8}\ \text{kg}^{-1}_{\text{cat}}\ \text{s}^{-1}$ for an active site density of $4.7 \times 10^{+18}\ \text{m}^{-2}$ and a specific surface area of $1.6 \times 10^{+5}\ \text{m}^2\ \text{kg}^{-1}_{\text{cat}}$. The lower value corresponds to mobile surface species with rotation and the upper value represents immobile

surface species without rotation. An intermediate value of $8.5 \times 10^{+6}$ $mol_{C_3H_8}$ kg_{cat}^{-1} s^{-1} is expected for mobile surface species without rotation.

Typical values for the activation energies in propane combustion reactions over oxide catalysts are reported to be in the range of 70–110 kJ mol^{-1} [9,13,56,57].

4. Experimental results: data treatment and effects of reaction conditions

Fig. 1a shows the propane conversion versus space time for different temperatures at $p_{C_3H_8,0} = 0.6$ kPa and $y_{O_2,0}y_{C_3H_8,0}^{-1} = 6.1$ $mol_{O_2,0}$ $mol_{C_3H_8,0}^{-1}$. Fig. 1b gives the propane conversion versus space time for different oxygen to propane inlet ratios at 595 K and $p_{C_3H_8,0} = 0.6$ kPa.

In order to obtain experimental partial reaction orders for propane and oxygen, a series of experiments with constant oxygen or propane inlet partial pressure is performed, as shown in Fig. 2a and b. This set of data is regressed with Eq. (4). The

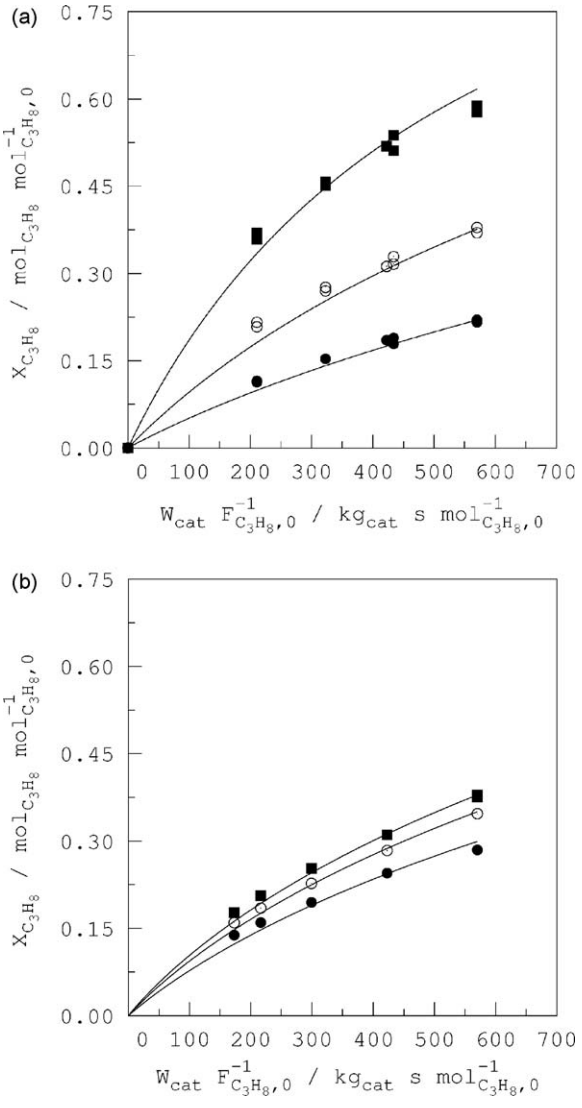

Fig. 1. Propane conversion versus space time at (a) $p_{C_3H_8,0} = 0.6$ kPa and $y_{O_2,0}y_{C_3H_8,0}^{-1} = 6.1$ $mol_{O_2,0}$ $mol_{C_3H_8,0}^{-1}$. (●) 595 K; (○) 621 K; (■) 648 K. (b) $p_{C_3H_8,0} = 1.0$ kPa and 595 K. (●) $y_{O_2,0}y_{C_3H_8,0}^{-1} = 6.1$ $mol_{O_2,0}$ $mol_{C_3H_8,0}^{-1}$; (○) $y_{O_2,0}y_{C_3H_8,0}^{-1} = 12.1$ $mol_{O_2,0}$ $mol_{C_3H_8,0}^{-1}$; (■) $y_{O_2,0}y_{C_3H_8,0}^{-1} = 18.0$ $mol_{O_2,0}$ $mol_{C_3H_8,0}^{-1}$. $p_{CO_2,0} = p_{H_2O,0} = 0.0$ kPa. Full lines were calculated with the parameter estimates for model LH*2, given in Table 3, by integration of Eq. (1) with Eq. (32).

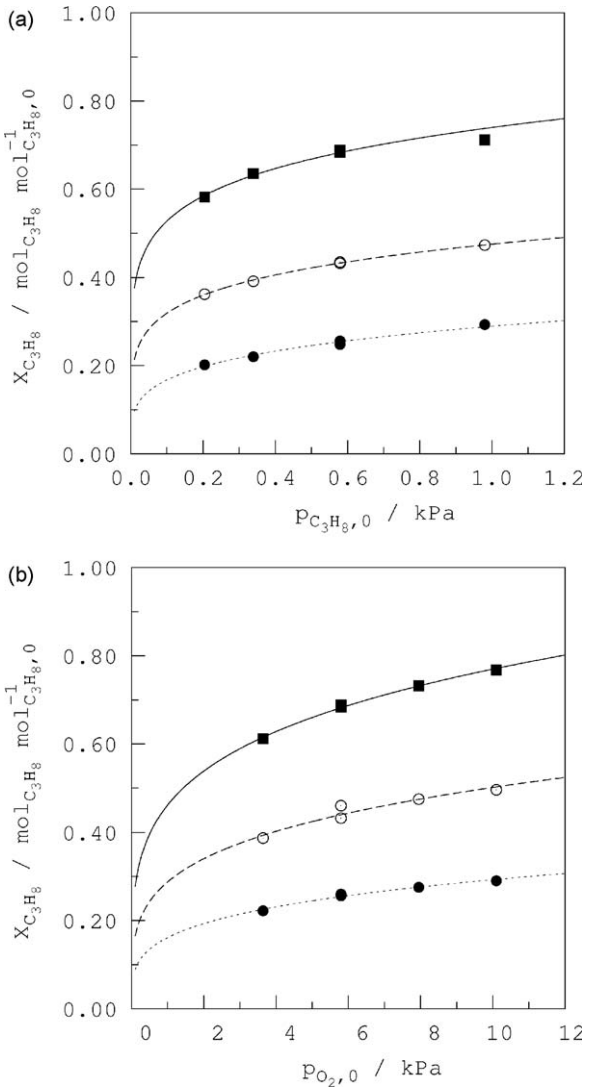

Fig. 2. (a) Propane conversion versus propane inlet partial pressure at $p_{O_2,0} = 5.8$ kPa. (b) Propane conversion versus oxygen inlet partial pressure at $p_{C_3H_8,0} = 0.6$ kPa. $W_{cat}F_{C_3H_8,0}^{-1} = 570$ kg_{cat} s $mol_{C_3H_8,0}^{-1}$ and $p_{CO_2,0} = p_{H_2O,0} = 0.0$ kPa. (●) 595 K; (○) 621 K; (■) 648 K. Lines are obtained by regression of the given experimental data by integration of Eq. (1) with Eq. (4). (. . . .) 595 K; (- - - -) 621 K; (– –) 648 K.

experimentally obtained partial reaction orders for propane and oxygen vary from 0.27 ± 0.05 and 0.25 ± 0.06 at 595 K to 0.21 ± 0.03 and 0.22 ± 0.02 at 648 K. Based on the 95% confidence intervals, it can be concluded that the obtained partial reaction orders are approximately independent of the reaction temperature.

The initial reaction rate for propane total oxidation versus the propane inlet partial pressure at $y_{O_2,0}y_{C_3H_8,0}^{-1} = 6.1$ $mol_{O_2,0}$ $mol_{C_3H_8,0}^{-1}$ is given in Fig. 3. An important property of the experimentally obtained initial reaction rate versus the inlet propane partial pressure, vide Section 5.2, is that a concave or at most a linear trend is observed over the applied experimental pressure range.

Fig. 4a and b shows the propane conversion versus space time at $y_{O_2,0}y_{C_3H_8,0}^{-1} = 6.1$ $mol_{O_2,0}mol_{C_3H_8,0}^{-1}$ and $T = 621$ K for an increasing water and carbon dioxide inlet partial pressure. Addition of water to the feed up to 5.5 kPa, vide Fig. 4a, causes a large decrease of the propane conversion. Doubling the water inlet partial pressure leads to a further, but less pronounced, decrease of the experimental propane conversion. On the other hand, the effect of carbon dioxide in the feed is less pronounced (vide Fig. 4b).

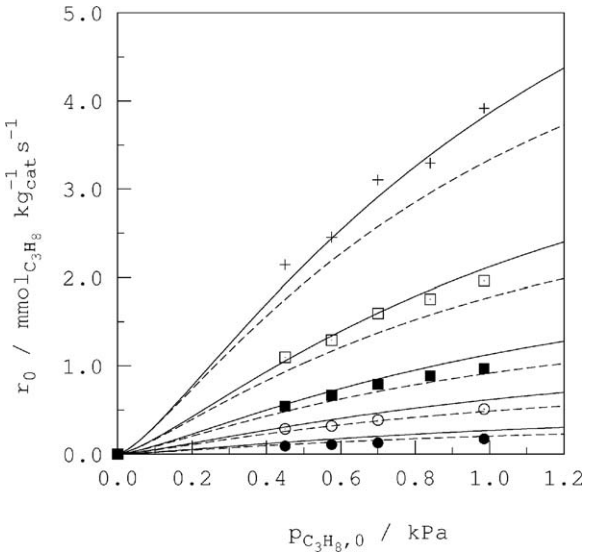

Fig. 3. Initial reaction rate versus propane inlet partial pressure at $y_{O_2,0}y_{C_3H_8,0}^{-1} = 6.1\ mol_{O_2,0}\ mol_{C_3H_8,0}^{-1}$ and $p_{CO_2,0} = p_{H_2O,0} = 0.0$ kPa. Experimental: (●) $T = 543$ K; (○) $T = 572$ K; (■) $T = 595$ K; (□) $T = 621$ K; (+) $T = 648$ K. Experimental rate data are obtained via Eqs. (1) and (2) at zero space time. Dashed lines were calculated with the parameter estimates for model LH18, given in Table 3, by integration of Eq. (1) with Eq. (28). Full lines were calculated with the parameter estimates for model LH*2, given in Table 3, by integration of Eq. (1) with Eq. (32).

5. Model discrimination

5.1. Reaction orders

It can be observed from the model equations given in Table S-3 that the oxygen partial reaction order ranges from −1 to 0 for models LH1 to LH3 and from −1/2 to 0 for models LH4 to LH6. The propane partial reaction order ranges from −1 to 0 for models LH7 to LH9 and from −2 to 0 for models LH10 to LH12. Since positive partial reaction orders for oxygen and propane are experimentally observed, vide Section 4, it can be concluded that the adsorption of one of the reactants cannot be the rate-determining step in the total oxidation of propane.

5.2. Initial rate analysis

The expected initial reaction rate versus the propane inlet partial pressure according to all ER models has a strictly positive second order derivative towards the propane inlet partial pressure, corresponding to a convex relation between the initial reaction rate and the propane inlet partial pressure. This is in contrast to the dependency, shown in Fig. 3, and all ER models can be excluded from the list of potential models. In the given experimental range, vide Table 1, all LH and MVK initial reaction rates show a linear to concave dependency and are further considered in the parameter estimation procedure. Also, the clear dependency of the experimental initial reaction rate on the propane inlet partial pressure justifies leaving out the possibility of the desorption of reaction products as the rate-determining step, vide Section 3.1.

5.3. Transformation procedure

The application of the procedure, proposed by Barnard and Mitchell [46,47], results in the rejection of all twenty competitive-adsorption rate expressions, vide Eq. (7), and the models MVK2, vide Eq. (12), MVK3, MVK4 and MVK6. Models LH13 to LH24, generally represented by Eq. (6), possess positive transformed-parameter values at every temperature level, from which the original kinetic parameters can be successfully calculated. These kinetic models represent the LH mechanism with the surface reaction as rate-determining step for molecular and dissociative adsorption of oxygen. One or two oxygen species are involved in the surface reaction and the fractional coverage of the reaction products is gradually taken into account, giving rise to $2 \times 2 \times 3 = 12$ models.

Models MVK1, vide Eq. (9), and MVK5, having positive transformed-parameter values, are generally capable to describe the experimental data, but when reaction products are explicitly added to the feed, the final rate expression should contain adsorption equilibrium coefficients. The former is the most common form of the MVK rate expression [9,11,14,58–60]. Typically, it has been applied to describe experimental data on oxidation kinetics, obtained without water or carbon dioxide in the feed. It should be noted that, applied to the subset of experiments, corresponding to feed without water or carbon dioxide, this

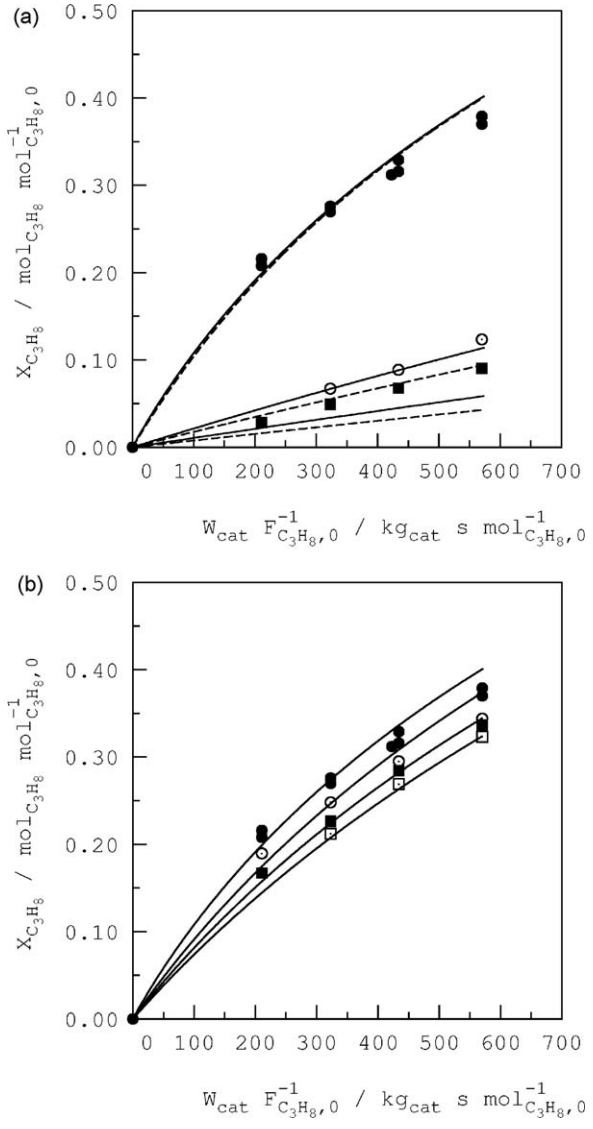

Fig. 4. Propane conversion versus space time at (a) $p_{O_2,0} = 0.0$ kPa and (●) $p_{H_2O,0} = 0.0$ kPa; (○) $p_{H_2O,0} = 5.5$ kPa; (■) $p_{H_2O,0} = 10.2$ kPa. Dashed lines were calculated with the parameter estimates for model LH18, given in Table 3, by integration of Eq. (1) with Eq. (28). (b) $p_{H_2O,0} = 0.0$ kPa and (●) $p_{CO_2,0} = 0.0$ kPa; (○) $p_{CO_2,0} = 4.1$ kPa; (■) $p_{CO_2,0} = 7.5$ kPa; (□) $p_{CO_2,0} = 11.9$ kPa. $p_{C_3H_8,0} = 0.6$ kPa, $y_{O_2,0}y_{C_3H_8,0}^{-1} = 6.1\ mol_{O_2,0}\ mol_{C_3H_8,0}^{-1}$ and 621 K. Full lines were calculated with the parameter estimates for model LH*2, given in Table 3, by integration of Eq. (1) with Eq. (32).

expression allows to describe this subset almost as well as the final model, selected in the present work. This is shown in Section S.6. However, as the given MVK models cannot explicitly account for water and carbon dioxide in the feed, vide Section 3.1.3, they are discarded from the list of possible models. For the same reason, models LH13, LH16, LH19 and LH22 are removed from the list. Since an explicit water and carbon dioxide partial pressure dependency is present in models MVK7 to MVK10, vide Table S-3, these rate expressions are taken along to the non-isothermal parameter estimation.

The isothermal results for model LH18 are shown in Fig. 5a and b. Similar diagrams are obtained for the other 11 remaining LH models. Linear relationships with multiple correlation coefficients above 0.90 are found for the surface reaction rate coefficient and the adsorption equilibrium coefficients of water and carbon dioxide. It can be observed from Fig. 5a that the adsorption equilibrium coefficients for oxygen and propane are nearly constant in the investigated experimental temperature range which is in line with the practically constant partial reaction orders, vide Section 4. From Fig. 5b it is observed that the temperature dependency in the van't Hoff relations for the adsorption equilibrium of water and carbon dioxide, vide Eq. (16), can be described properly. The obtained Arrhenius diagrams for the remaining LH models provide initial guesses for the preexponential factors, activation energies and reaction enthalpies in the non-isothermal regression procedure, in which all experimental data are treated simultaneously.

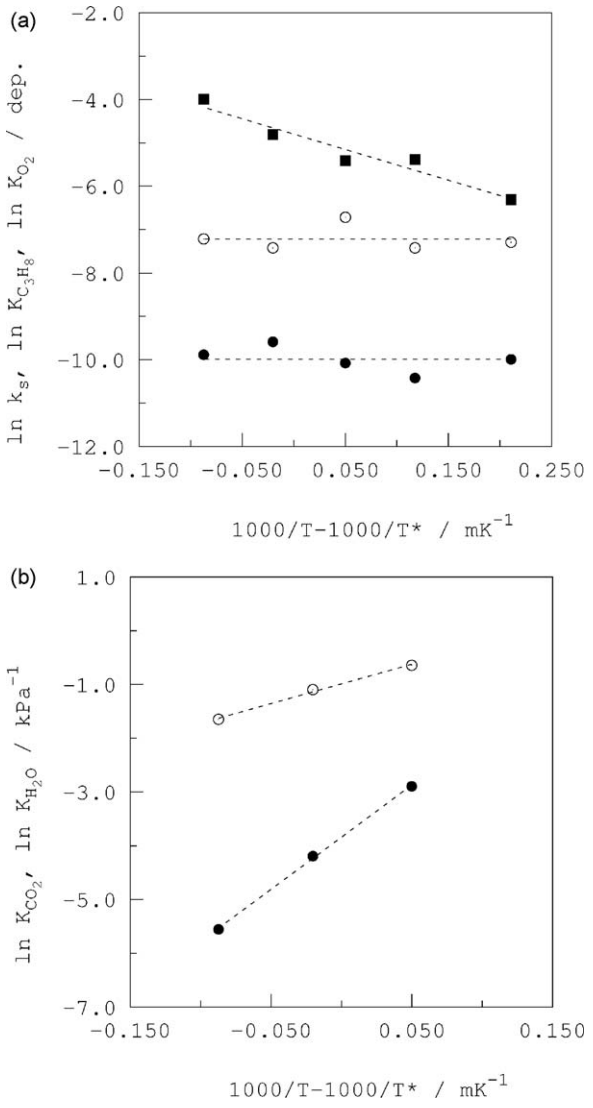

Fig. 5. Isothermal parameter estimates as a function of the inverse of the temperature corrected for the average temeprature T*, obtained from minimization of Eq. (17), applied for model LH18, vide Eq. (28). (a) (■) k_s; (●) K_{O_2}; (○) $K_{C_3H_8}$. (b) (●) K_{CO_2}; (○) K_{H_2O}. The dashed lines are only shown to guide the eye.

5.4. Non-isothermal parameter estimation

Table 3 gives the obtained parameter estimates from the weighted non-isothermal regression analysis for model LH18, vide Eq. (28). The corresponding elementary steps are listed in Table 2. The information for the parameter estimates corresponding to the other LH models is given in Table S-5 vide section S.6. Unless specified otherwise, the conclusions on these estimates correspond to those of model LH18.

$$r = k_s \frac{\sqrt{K_{O_2} p_{O_2}} K_{C_3H_8} p_{C_3H_8}}{\left(1 + \sqrt{K_{O_2} p_{O_2}} + K_{C_3H_8} p_{C_3H_8} + K_{H_2O} p_{H_2O} + K_{CO_2} p_{CO_2}\right)^2} \quad (28)$$

The reported estimates differ at most 15% from the initial guesses, obtained from the transformation procedure, indicating the relevance and applicability of this procedure. It is observed from Table 3 that the order of magnitude of the preexponential factor corresponds to the range given by Dumesic et al. [55], vide Section 3.2.4: the actual surface species in the total oxidation of propane over CuO-CeO_2/γ-Al_2O_3 are mobile species with rotation. Estimated activation energies are within the expected range, vide Section 3.2.4.

The temperature dependency of the adsorption coefficients for propane and oxygen cannot be estimated significantly, as expected from isothermal regression results and the experimentally obtained reaction orders, vide Section 4. Adsorption enthalpies for water and carbon dioxide can be significantly estimated. The estimated adsorption entropies satisfy Eq. (26) for all models. Although the propane adsorption enthalpy cannot be significantly estimated, Eq. (27) is fulfilled. For the oxygen adsorption enthalpy, values ranging from 37 to 97 kJ mol^{-1} are reported in literature [13] and, hence, the estimated oxygen adsorption enthalpies meet Eq. (27). For the adsorption parameters of water and carbon dioxide, Eqs. (26) and (27) are satisfied within the 95% confidence intervals. This is not uncommon for estimated adsorption parameters [61–63].

Application of the likelihood-ratio criterion, vide Section 3.2.3, to the 12 competitive LH models results in the selection of model LH18, vide Eq. (28), which can describe the experimental data best: this model has the lowest RSSQ and the highest F value for the global significance of the regression. The highest binary correlation coefficient between the estimated parameters amounts to 0.87 and is found between the activation energy of the surface reaction and the adsorption enthalpy of carbon dioxide. Hence, significant correlation within the set of parameters can be ruled out for the selected model. Moreover, the selected model is found to be the only adequate one with a calculated $(F_{LH18})_{ad,calc}$ value for the model adequacy of 1.61, which is below the tabulated value of 1.68 [49].

Fig. 3 shows experimental reaction rate data versus propane inlet partial pressure for five reaction temperatures. The simulated reaction rate data show a good agreement with the experimental data for low temperatures. However, for higher reaction temperatures a tendency to underestimate the experimental data is observed. A similar observation holds for Fig. 4a: the higher the water inlet partial pressure, the larger the difference in model calculated propane conversion and the experimentally obtained

value. These data can be considered as co-adsorption experiments between propane and water, since these components were both present in the reactor feed, vide Section S.7.

In order to obtain a less pronounced decrease of the oxidation rate with increasing water inlet partial pressure, model refinement with respect to the adsorption behaviour of water is performed to overcome this tendency, vide Section 6. The latter can be obtained by considering a more detailed interaction between oxygen and water derived surface species, all of them considered to be quasi-equilibrated.

6. Model refinement

6.1. Kinetic models

Table 2 lists the elementary steps for refined model LH*2. Other possible refined reaction paths, based on elementary steps, and the corresponding rate expressions are given in Tables S-7 and S-8, vide section S.8. Reaction path LH*2 assumes a disproportionation reaction, vide step 5 in Table 2, in which two surface hydroxyl species can form a molecularly adsorbed water species and an adsorbed oxygen species. More information on this reaction can be found in Section S.9. From the equilibrium relations corresponding to steps 2, 4 and 5, vide Table 2, Eq. (29) is obtained and the fractional coverage of hydroxyl species is given by Eq. (30).

$$K_{H_2O}K_{diss,2} = \frac{\theta_{HO^*}^2}{p_{H_2O}\sqrt{K_{O_2}\,p_{O_2}}\,\theta_*^2} \tag{29}$$

$$\theta_{HO^*} = \sqrt{K_{H_2O}K_{diss,2}\,p_{H_2O}}\,\sqrt[4]{K_{O_2}\,p_{O_2}}\,\theta_* \tag{30}$$

With the quasi-equilibrated steps 1, 2, 4 and 6, the rate-determining surface reaction step 3, Eq. (30) and the balance for active sites, vide Eq. (31), the reaction rate corresponding to reaction path LH*2 is obtained, vide Eq. (32). Other rate expressions for refined kinetic models, vide Table S-8, are obtained in an analogous way.

$$\theta_* + \theta_{C_3H_8^*} + \theta_{O^*} + \theta_{CO_2^*} + \theta_{H_2O^*} + \theta_{HO^*} = 1 \tag{31}$$

$$r = k_s \frac{K_{C_3H_8}\,p_{C_3H_8}\sqrt{K_{O_2}\,p_{O_2}}}{\left(1 + K_{C_3H_8}\,p_{C_3H_8} + \sqrt{K_{O_2}\,p_{O_2}} + K_{H_2O}\,p_{H_2O} + \sqrt{K_{H_2O}K_{diss,2}\,p_{H_2O}}\,\sqrt[4]{K_{O_2}\,p_{O_2}} + K_{CO_2}\,p_{CO_2}\right)^2} \tag{32}$$

Fractional coverages for adsorbed propane, dissociatively chemisorbed oxygen, carbon dioxide, water and hydroxyl species are given by Eqs. (33)–(37), with N_{LH^*2} the square root of the denominator in Eq. (32). The fractional coverage for the free active sites is obtained by solving Eq. (31) for θ_* and subsequent substitution of Eqs. (33)–(37):

$$\theta_{C_3H_8^*} = \frac{K_{C_3H_8}\,p_{C_3H_8}}{N_{LH^*2}} \tag{33}$$

$$\theta_{O^*} = \frac{\sqrt{K_{O_2}\,p_{O_2}}}{N_{LH^*2}} \tag{34}$$

$$\theta_{CO_2^*} = \frac{K_{CO_2}\,p_{CO_2}}{N_{LH^*2}} \tag{35}$$

Table 3
Parameter estimates with their 95% confidence intervals obtained by regression of the experimental data, vide Table 1, with Eq. (1) and the kinetic models LH18, vide Eq. (28), and LH*2, vide Eq. (32). $F_{sig,tab} = 3.36$; $F_{ad,tab} = 1.68$.

Parameter	Unit	LH18	LH*2
$k_{s,0}$	$/10^{+4}$ mol kg_{cat}^{-1} s^{-1}	12.1 ± 4.9	9.6 ± 1.1
E_A	/kJ mol^{-1}	78.0 ± 5.7	74.4 ± 4.6
$-\Delta S^\circ_{O_2}$	/J mol^{-1} K^{-1}	91.2 ± 1.4	97.7 ± 5.6
$-\Delta H^\circ_{O_2}$	/kJ mol^{-1}	0.0 [a]	0.0 [a]
$-\Delta S^\circ_{C_2H_8}$	/J mol^{-1} K^{-1}	60.8 ± 1.4	61.7 ± 0.4
$-\Delta H^\circ_{C_2H_8}$	/kJ mol^{-1}	0.0[a]	0.0[a]
$-\Delta S^\circ_{H_2O}$	/J mol^{-1} K^{-1}	185.5 ± 19.6	154.2 ± 23.3
$-\Delta H^\circ_{H_2O}$	/kJ mol^{-1}	75.6 ± 12.2	53.8 ± 20.0
$-\Delta S^\circ_{CO_2}$	/J mol^{-1} K^{-1}	190.0 ± 1.6	173.3 ± 37.9
$-\Delta H^\circ_{CO_2}$	/kJ mol^{-1}	64.5 ± 26.2	54.2 ± 23.7
$-\Delta S^\circ_{diss,2}$	/J mol^{-1} K^{-1}	–	156.5 ± 11.2
$-\Delta H^\circ_{diss,2}$	/kJ mol^{-1}	–	99.1 ± 10.8
S_m	/mol^2 mol^{-2}	1.20	1.11
$(F_m)_{sig,\ calc}$	/–	13239	11805
$(F_m)_{ad,\ calc}$	/–	1.61	1.54
$\lvert\rho_{max}\rvert$	/–	0.87	0.84

[a] Parameter cannot be estimated significantly.

$$\theta_{H_2O^*} = \frac{K_{H_2O}\,p_{H_2O}}{N_{LH^*2}} \tag{36}$$

$$\theta_{HO^*} = \frac{\sqrt{K_{H_2O}K_{diss,2}\,p_{H_2O}}\,\sqrt[4]{K_{O_2}\,p_{O_2}}}{N_{LH^*2}} \tag{37}$$

It has to be noted that the theoretical partial reaction orders obtained on the additionally proposed models are not in conflict with earlier made conclusions, vide Section 5.1. Also, these models have the same characteristics in initial reaction rate versus propane inlet partial pressure. Hence, it is assumed that this model refinement will not affect the outcome of the transformation procedure as well as the discrimination procedure, vide Section 5.2.

6.1.1. Kinetic parameters in the model refinement: non-isothermal estimation and assessment

The results from the non-linear parameter estimation for model LH*2, vide Eq. (32), are given in Table 3. The results for the other refined models can be found in Table 3. The estimated preexponential factor and the activation energy as well as the adsorption entropies for propane, oxygen and carbon dioxide correspond with the values of model LH18. The parameters for the molecular adsorption of water are somewhat lower: K_{H_2O} is calculated as $5.1 \pm 0.5 \times 10^{-4}$ kPa^{-1} for model LH18 and as $3.2 \pm 0.6 \times 10^{-4}$ kPa^{-1} for model LH*2 at $T^* = 617$ K. Since the corresponding Gibbs free energy becomes negative at 349 K, the equilibrium for step 4, vide Table 2, is shifted to the right for all reaction temperatures. The parameter estimates for the surface disproportionation of two hydroxyl species into a molecularly adsorbed water species and a dissociatively adsorbed oxygen species, vide step 5 in Table 2, are physically meaningful. Shustorovich and Sellers [64] report it as endothermic and the entropy change is positive, i.e., a surface oxygen species and a surface water species possess more entropy than two surface hydroxyl groups. $K_{diss,2}$ equals unity at 633 K and the surface disproportionation reaction is favored at high temperatures, whereas the surface comproportionation reaction, which is the reverse of a disproportionation reaction, takes place at lower temperatures.

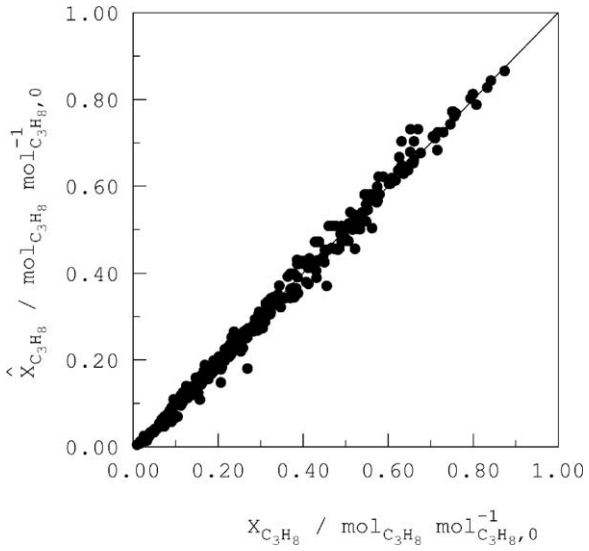

Fig. 6. Calculated versus experimental propane conversion, obtained from integration of Eq. (1) with Eq. (32), and the corresponding parameter estimates for model LH*2, given in Table 3. Experimental conditions are given in Table 1.

From the list of proposed refined reaction paths, vide Section S.8, model LH*2 provides the lowest RSSQ and the highest value for the global significance of the regression, vide Section S.10. This model describes the experimental data adequately: the calculated $(F_{LH^*2})_{ad,calc}$ value is 1.54, vide Eq. (23), whereas the tabulated value $(F_{LH^*2})_{ad,tab}(10,367;\ 0.95)$ is 1.68. A maximum correlation coefficient of 0.84 between the activation energy for the surface reaction and the adsorption enthalpy for carbon dioxide is observed, and hence, significant correlation between the kinetic parameters is ruled out.

From Fig. 3, it is observed that the simulation of experimental initial rate data with model LH*2 shows better agreement than when model LH18 is used, especially the data on higher reaction temperatures. Also, better model calculations are obtained for the experimental data with water in the feed, shown in Fig. 4a. The parity diagram, corresponding to model LH*2, is given in Fig. 6. For the whole experimental range, the model based calculated propane conversion shows good agreement with the corresponding experimental value.

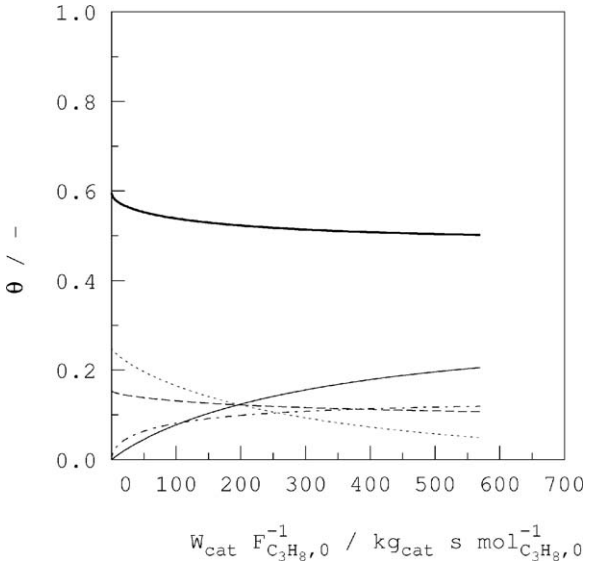

Fig. 7. Fractional coverages versus space time at $p_{C_3H_8,0} = 0.7$ kPa, $y_{O_2,0}y^{-1}_{C_3H_8,0} = 12.1\ mol_{O_2,0}\ mol^{-1}_{C_3H_8,0}$, $p_{CO_2,0} = p_{H_2O,0} = 0.0$ kPa and $T = 648$ K. (...) $\theta_{C_3H_8}$; (- - - -) θ_{O^*}; (––) $\theta_{H_2O^*}$; (-. -. -.) θ_{HO^*}; (–––) θ_*. Lines are obtained from Eqs. (33), (34), (36), and (37) using the partial pressure profiles obtained after integration of Eq. (1) with Eq. (32) and the corresponding parameter estimates for model LH*2, vide Table 3. The fractional coverage for the free active sites is obtained by solving Eq. (31) for θ_* and subsequent substitution of Eqs. (33)–(37).

Fractional coverages, corresponding to model LH*2, at $p_{C_3H_8,0} = 0.7$ kPa, $y_{O_2,0}y^{-1}_{C_3H_8,0} = 12.1\ mol_{O_2,0}\ mol^{-1}_{C_3H_8,0}$, $p_{CO_2,0} = p_{H_2O,0} = 0.0$ kPa and $T = 648$ K through the reactor up to $W_{cat}F^{-1}_{C_3H_8,0} = 570\ kg_{cat}\ s\ mol^{-1}_{C_3H_8,0}$ are shown in Fig. 7. As the propane conversion increases through the catalyst bed, the corresponding fractional coverage decreases, vide Eq. (33), whereas the fractional coverage for oxygen and the free active sites decrease more moderately. At the given conditions, the fraction of free sites is approximately 0.55.The fractional coverage of water and hydroxyl species increases, since the former is formed by reaction and the latter is in equilibrium with the former by elementary step 5, vide Table 2. The fractional coverage for carbon dioxide never exceeds 0.02 (not shown).

Fractional coverages are calculated for different water inlet partial pressures at $p_{C_3H_8,0} = 0.7$ kPa, $y_{O_2,0}y^{-1}_{C_3H_8,0} = 12.1\ mol_{O_2,0}\ mol^{-1}_{C_3H_8,0}$ and $W_{cat}F^{-1}_{C_3H_8,0} = 570\ kg_{cat}\ s\ mol^{-1}_{C_3H_8,0}$. Fig. 8a–d shows the fractional coverages at the reactor outlet versus reaction temperature. From Fig. 8a it is observed that at least 20% of the catalyst surface is free during reaction. At the highest reaction temperature this fraction is more than doubled. The surface hydroxyl fractional coverage decreases rapidly when the reaction temperature increases, which is expected from $K_{diss,2}$, for which disproportionation is favored at higher temperatures, vide Table 3. The propane fractional coverage shows a maximum of 0.20 and decreases rapidly to zero for a temperature higher than 550 K, whereas the fractional oxygen surface coverage remains more or less constant. A maximum of 0.20 for the fractional coverage of water is observed: when the temperature increases first more water is produced by reaction and stays adsorbed on the catalyst surface. When the temperature further increases, the water desorption becomes more pronounced and overcompensates the production by reaction.

When water is added to the reactor inlet, it can be observed from Fig. 8b–d that practically no free active sites are present at 450 K. For higher temperatures this fraction increases, since the equilibrium for the desorption of the reaction products is towards the side of the desorbed products. The maximum in the propane fractional coverage shifts towards higher temperatures, in the case the water inlet partial pressure increases. The basis for this observation is the competitive adsorption between water and propane. The oxygen fractional coverage is approximately zero at 450 K, after which it increases practically linearly. For the hydroxyl fractional surface coverage, a rapid decrease is observed, similar as for the case without water in the feed. At 450 K, the calculated water surface fractional coverage increases from 20%, for $p_{H_2O,0} = 0.0$ kPa, to 35%, for $p_{H_2O,0} = 10.0$ kPa. As the temperature increases, the water surface fractional coverage shows two maxima, although less pronounced with increasing water inlet partial pressure. The maximum around 550 K originates from the equilibrium in elementary step 4, vide Table 2, in which gas phase water is in equilibrium with surface water species, arising from propane total oxidation reaction as well as adsorption from the gas phase. The maximum around 650 K is explained by the behaviour of $K_{diss,2}$: the higher the reaction temperature, the more the equilibrium of step 5, vide Table 2, shifts towards disproportionation of the surface hydroxyl species, giving rise to a higher fractional coverage of water species. The additional production is tempered by the

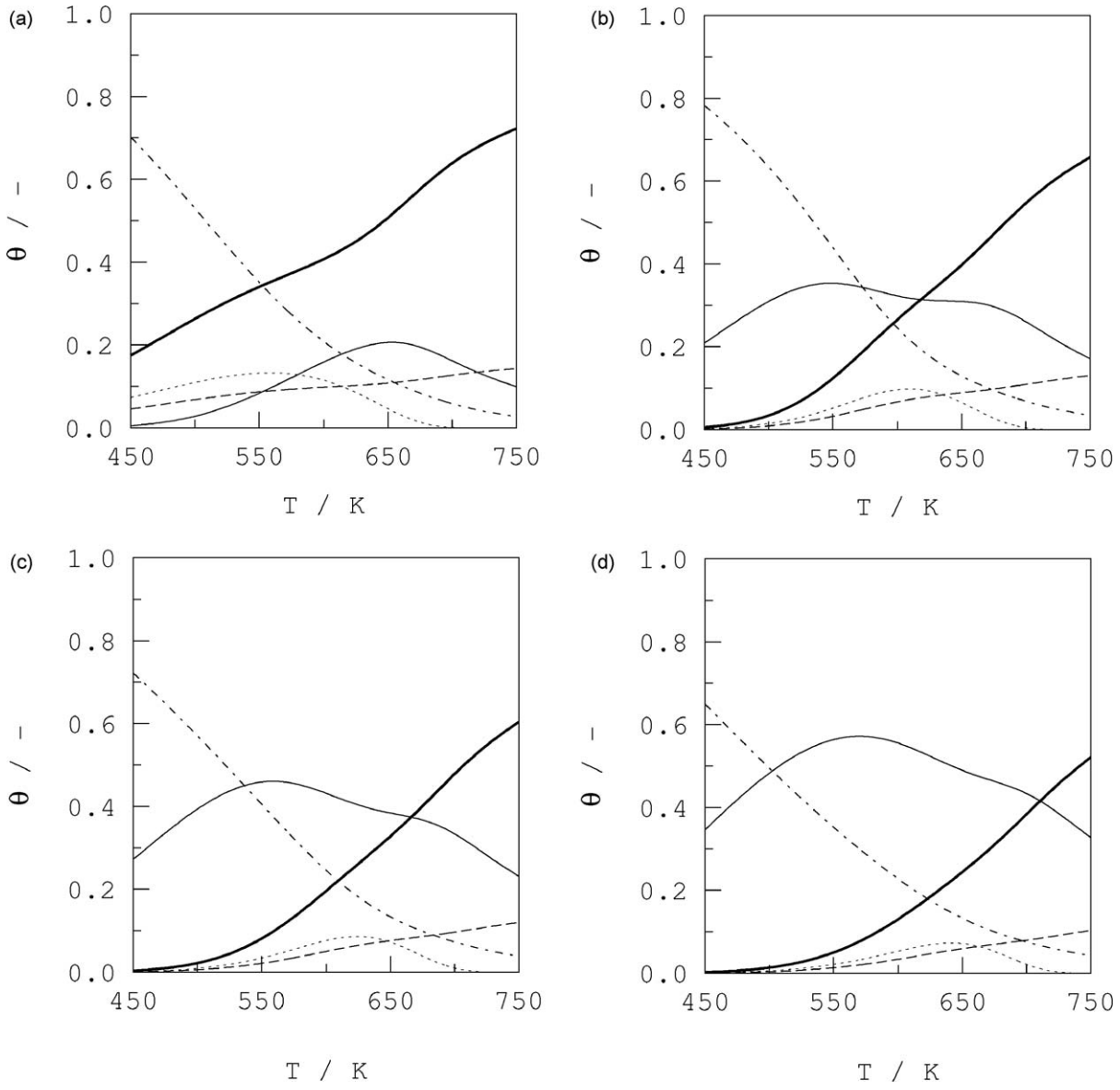

Fig. 8. Fractional coverages versus temperature at $p_{C_3H_8,0} = 0.7\,\text{kPa}$, $y_{O_2,0}y^{-1}_{C_3H_8,0} = 12.1\,\text{mol}_{O_2,0}\,\text{mol}^{-1}_{C_3H_8,0}$, $p_{CO_2,0} = 0.0\,\text{kPa}$ and $W_{cat}F^{-1}_{C_3H_8,0} = 570\,\text{kg}_{cat}\,\text{s}\,\text{mol}^{-1}_{C_3H_8,0}$. (a) $p_{H_2O,0} = 0.0\,\text{kPa}$; (b) $p_{H_2O,0} = 2.5\,\text{kPa}$; (c) $p_{H_2O,0} = 5.0\,\text{kPa}$; (d) $p_{H_2O,0} = 10.0\,\text{kPa}$. (. . .) $\theta_{C_3H_8^*}$; (- - - -) θ_{O^*}; (––) $\theta_{H_2O^*}$; (-. -. -. -) θ_{HO^*}; (–––) θ_*. Lines are obtained from Eqs. (33), (34), (36) and (37) using the partial pressure profiles obtained after integration of Eq. (1) with Eq. (32) and the corresponding parameter estimates for model LH*2, vide Table 3. The fractional coverage for the free active sites is obtained by solving Eq. (31) for θ_* and subsequent substitution of Eqs. (33)–(37).

equilibrium with the gas phase, and hence, the fractional coverage again decreases for higher temperatures. Since no water is added to the feed, the first maximum is not significantly observed in Fig. 8a. Typical industrial inlet conditions contain 0.10 $\text{mol}_{H_2O,0}\,\text{mol}^{-1}_{t,0}$ water in the feed. At these conditions, approximately half of the catalyst surface is covered with water.

7. Conclusions

In the presence of water and carbon dioxide, the propane total oxidation kinetics over CuO-CeO_2/γ-Al_2O_3 can be most adequately described using a Langmuir–Hinshelwood type of rate equation. The corresponding reaction mechanism considers the surface reaction as the rate-determining step, in which dissociatively chemisorbed oxygen reacts with adsorbed propane. Molecular water adsorption on the catalytic surface is followed by a dissociation reaction in which water interacts with a dissociatively adsorbed oxygen species to form two hydroxyl species. All adsorption steps in the proposed reaction mechanism, including the molecular adsorption of carbon dioxide, can be considered to be quasi-equilibrated. The corresponding kinetic model describes the experimental data better than the model with only the molecular adsorption equilibrium for water.

Small amounts of water, added to the feed, have a significant negative effect on the total oxidation rate of propane. As the water inlet partial pressures further increases, this negative effect is more moderate. At typical operating conditions, the catalyst surface is mainly covered with water and hydroxyl species, while the fractional coverage of propane and oxygen never exceeds 0.15. For typical industrial inlet conditions, having 0.10 $\text{mol}_{H_2O,0}\,\text{mol}^{-1}_{t,0}$ water in the feed, approximately half of the catalyst surface is covered with water. The effect of carbon dioxide in the feed on the total oxidation rate of propane is far less pronounced than the effect of water in the feed.

Acknowledgements

This work was performed in the framework of a Concerted Research Action (GOA), financed by Ghent University. Part of this research was carried out within the framework of the Interuniversity Attraction Poles Programme funded by the Belgian Science Policy.

Appendix A. Supplementary data

Supplementary data associated with this article can be found, in the online version, at doi:10.1016/j.apcatb.2009.11.018.

References

[1] J. Theloke, R. Friedrich, Atmos. Environ. 41 (2007) 4148–4160.
[2] J.J. Spivey, Ind. Eng. Chem. Res. 26 (1987) 2165–2180.
[3] M. Zimowska, A. Michalik-Zym, R. Janik, T. Machej, J. Gurgul, R.P. Socha, J. Podobinski, E.M. Serwicka, Catal. Today 119 (2007) 321–326.
[4] A.C. Gluhoi, N. Bogdanchikova, B.E. Nieuwenhuys, Catal. Today 113 (2006) 178–181.
[5] B. Solsona, T.E. Davies, T. Garcia, I. Vazquez, A. Dejoz, S.H. Taylor, Appl. Catal., B: Environ. 84 (2008) 176–184.
[6] B. Solsona, T. Blasco, J.M.L. Nieto, M.L. Pena, F. Rey, A. Vidal-Moya, J. Catal. 203 (2001) 443–452.
[7] R. Auer, F.C. Thyrion, Ind. Eng. Chem. Res. 41 (2002) 680–690.
[8] A. Bampenrat, V. Meeyoo, B. Kitiyanan, P. Rangsunvigit, T. Rirksomboon, Catal. Commun. 9 (2008) 2349–2352.
[9] P.M. Heynderickx, J.W. Thybaut, H. Poelman, D. Poelman, G.B. Marin, Appl. Catal., B: Environ. 90 (2009) 295–306.
[10] L.Y. Hsu, H.S. Teng, Appl. Catal., B: Environ. 35 (2001) 21–30.
[11] B.Y. Jibril, S.M. Al-Zahrani, A.E. Abasaeed, R. Hughes, Chem. Eng. J. 103 (2004) 59–67.
[12] L. Late, E.A. Blekkan, J. Nat. Gas Chem. 11 (2002) 33–42.
[13] K.S. Song, D. Klvana, J. Kirchnerova, Appl. Catal., A: Gen. 213 (2001) 113–121.
[14] T.K. Tseng, H. Chu, T.H. Ko, L.K. Chaung, Chemosphere 61 (2005) 469–477.
[15] G. Ertl, H. Knözinger, J. Weitkamp, Preparation of Solid Catalysts, Wiley-VCH, Weinheim, 1999.
[16] J.A. Schwarz, C. Contescu, A. Contescu, Chem. Rev. 95 (1995) 477–510.
[17] G.F. Froment, K.B. Bischoff, Chemical Reactor Analysis and Design, 2nd ed., Wiley, New York, 1990.
[18] R.J. Berger, E.H. Stitt, G.B. Marin, F. Kapteijn, J.A. Moulijn, Cattech 5 (2001) 30–60.
[19] D. Klvana, J. Vaillancourt, J. Kirchnerova, J. Chaouki, Appl. Catal., A: Gen. 109 (1994) 181–193.
[20] G.F. Froment, K.B. Bischoff, Chemical Reactor Analysis and Design, 2nd Ed., Wiley, New York, 1990.
[21] G.F. Froment, L.H. Hosten, in: J.R. Anderson, M. Boudart (Eds.), Catal. Sci. Tech., Springer-Verlag, Berlin, 1981, pp. 97–170.
[22] I. Chorkendorff, J.W. Niemantsverdriet, Concepts of Modern Catalysis and Kinetics, 2nd ed., Wiley-VCH, Weinheim, 2007.
[23] A. Kaddouri, React. Kinet. Catal. Lett. 82 (2004) 401–409.
[24] G. Centi, F. Cavani, F. Trifiro, Selective Oxidation by Heterogeneous Catalysis, Kluwer Academic/Plenum Publishers, New York, 2001.
[25] E. Finocchio, G. Busca, V. Lorenzelli, R.J. Willey, J. Catal. 151 (1995) 204–215.
[26] E.A. Mamedov, V.C. Corberan, Appl. Catal., A: Gen. 127 (1995) 1–40.
[27] M.D. Amiridis, J.E. Rekoske, J.A. Dumesic, D.F. Rudd, N.D. Spencer, C.J. Pereira, AlChE J. 37 (1991) 87–97.
[28] F. Arena, F. Frusteri, A. Mezzapica, A. Parmaliana, Stud. Surf. Sci. Catal. 130 (2000) 3585–3590.
[29] F. Arena, F. Frusteri, A. Parmaliana, Appl. Catal., A: Gen. 197 (2000) 239–246.
[30] F. Arena, F. Frusteri, A. Parmaliana, AlChE J. 46 (2000) 2285–2294.
[31] F. Arena, N. Giordano, A. Parmaliana, J. Catal. 167 (1997) 66–76.
[32] R. Burch, D.J. Crittle, M.J. Hayes, Catal. Today 47 (1999) 229–234.
[33] R. Burch, M.J. Hayes, J. Mol. Catal. A: Chem. 100 (1995) 13–33.
[34] G. Busca, E. Finocchio, V. Lorenzelli, G. Ramis, M. Baldi, Catal. Today 49 (1999) 453–465.
[35] A. Parmaliana, F. Arena, J. Catal. 167 (1997) 57–65.
[36] Q. Sun, J.I. Dicosimo, R.G. Herman, K. Klier, M.M. Bhasin, Catal. Lett. 15 (1992) 371–376.
[37] P. Hurtado, S. Ordonez, H. Sastre, F.V. Diez, Appl. Catal., B: Environ. 51 (2004) 229–238.
[38] M.A. Vannice, Kinetics of Catalytic Reactions, Springer, New York, 2005.
[39] R. Auer, M. Alifanti, B. Delmon, F.C. Thyrion, Appl. Catal., B: Environ. 39 (2002) 311–318.
[41] P. Mars, D.W. van Krevelen, Chem. Eng. Sci. 3 (1954) 41–58.
[42] A.A. Barresi, G. Baldi, Chem. Eng. Sci. 47 (1992) 1943–1953.
[43] A.A. Barresi, I. Mazzarino, G. Baldi, Can. J. Chem. Eng. 70 (1992) 286–293.
[44] P. Hurtado, S. Ordoñez, H. Sastre, F.V. Diez, Appl. Catal., B: Environ. 51 (2004) 229–238.
[45] S. Ordoñez, L. Bello, H. Sastre, R. Rosal, F.V. Diez, Appl. Catal., B: Environ. 38 (2002) 139–149.
[46] J.A. Barnard, D.S. Mitchell, J. Catal. 12 (1968) 376–385.
[47] J.A. Barnard, D.S. Mitchell, J. Catal. 12 (1968) 386–397.
[48] P.T. Wierzchowski, L.W. Zatorski, Appl. Catal., B: Environ. 44 (2003) 53–65.
[49] D.M. Himmelblau, Process Analysis by Statistical Methods, Wiley, New York, 1970.
[50] D.W. Marquardt, J. Soc. Ind. Appl. Math. 11 (1963) 431–443.
[51] G.A.F. Seber, A.J. Lee, Linear Regression Analysis, 2nd ed., Wiley-Interscience, Hoboken, NJ, 2003.
[52] M.A. Vannice, S.H. Hyun, B. Kalpakci, W.C. Liauh, J. Catal. 56 (1979) 358–362.
[53] M. Boudart, D.E. Mears, M.A. Vannice, Ind. Chim. Belg. 32 (1967) 281–284.
[54] R.H. Perry, D.W. Green, J.O. Maloney, Perry's Chemical Engineers' Handbook, 7th ed., McGraw-Hill, New York, 1997.
[55] J.A. Dumesic, D.F. Rudd, L.M. Aparicio, J.E. Rekoske, A.A. Trevino, The Microkinetics of Heterogeneous Catalysis, American Chemical Society, Washington, DC, 1993.
[56] M. Baldi, E. Finocchio, F. Milella, G. Busca, Appl. Catal., B: Environ. 16 (1998) 43–51.
[57] K. Otto, J.M. Andino, C.L. Parks, J. Catal. 131 (1991) 243–251.
[58] K. Scheurell, E. Hoppe, K.W. Brzezinka, E. Kemnitz, J. Mater. Chem. 14 (2004) 2560–2568.
[59] C.H. Wang, S.S. Lin, H.S. Weng, J. Environ. Sci. Health. Part A Toxic/Hazard. Subst. Environ. Eng. 37 (2002) 1649–1663.
[60] V.R. Choudhary, G.M. Deshmukh, Chem. Eng. Sci. 60 (2005) 1575–1581.
[61] H. Backman, A.K. Neyestanaki, D.Y. Murzin, J. Catal. 233 (2005) 109–118.
[62] S. Smeds, D. Murzin, T. Salmi, Appl. Catal., A: Gen. 125 (1995) 271–291.
[63] W. Zhu, F. Kapteijn, B. van der Linden, J.A. Moulijn, Phys. Chem. Chem. Phys. 3 (2001) 1755–1761.
[64] E. Shustorovich, H. Sellers, Surf. Sci. Rep. 31 (1998) 5–119.
[65] R.J. Berger, J. Perez-Ramirez, F. Kapteijn, J.A. Moulijn, Chem. Eng. Sci. 57 (2002) 4921–4932.
[66] G.F. Froment, L.H. Hosten, in: J.R. Anderson, M. Boudart (Eds.), Catal.-Sci. Tech., Springer-Verlag, Berlin, 1981, pp. 97–170.
[67] H. Gierman, Appl. Catal. 43 (1988) 277–286.
[68] D.E. Mears, Chem. Eng. Sci. 26 (1971) 1361–1366.
[69] C. Perego, S. Peratello, Catal. Today 52 (1999) 133–145.
[70] D.L. Massart, Handbook of Chemometrics and Qualimetrics, Elsevier, Amsterdam, 1997.
[71] M. Egashira, S. Kawasumi, S. Kagawa, T. Seiyama, Bull. Chem. Soc. Jpn. 51 (1978) 3144–3149.
[72] O. Thinon, K. Rachedi, F. Diehl, P. Avenier, Y. Schuurman, Top. Catal. 14 (2009) 1–6.
[73] D. Ciuparu, N. Katsikis, L. Pfefferle, Appl. Catal., A: Gen. 216 (2001) 209–215.
[74] D. Ciuparu, L. Pfefferle, Appl. Catal., A: Gen. 209 (2001) 415–428.
[75] T.J. Toops, A.B. Walters, M.A. Vannice, Appl. Catal., B: Environ. 38 (2002) 183–199.
[76] T.J. Toops, A.B. Walters, M.A. Vannice, Appl. Catal., A: Gen. 233 (2002) 125–140.
[77] T.J. Toops, A.B. Walters, M.A. Vannice, Catal. Lett. 82 (2002) 45–57.
[78] K.D. Chen, E. Iglesia, A.T. Bell, J. Catal. 192 (2000) 197–203.
[79] K.D. Chen, A. Khodakov, J. Yang, A.T. Bell, E. Iglesia, J. Catal. 186 (1999) 325–333.
[80] E. Heracleous, A.A. Lemonidou, J. Catal. 237 (2006) 175–189.
[81] S. Pietrzyk, M. Mahmoud, T. Rembeczky, R. Bechara, M. Czernicki, N. Fatah, in: G.F. Froment, K.C. Waught (Eds.), International Symposium on Dynamics of Surfaces and Reaction Kinetics in Heterogeneous Catalysis, Elsevier Science Publication, Antwerp, Belgium, 1997, pp. 263–271.
[82] C.L. Zhao, I.E. Wachs, Catal. Today 118 (2006) 332–343.
[83] E. Tserpe, K.C. Waugh, Stud. Surf. Sci. Catal. 109 (1997) 401–416.